PHYSICAL REVIEW B **95**, 094420 (2017)

Single-component molecular material hosting antiferromagnetic and spin-gapped Mott subsystems

Rina Takagi,[1] Takamasa Hamai,[1] Hiro Gangi,[1] Kazuya Miyagawa,[1] Biao Zhou,[2] Akiko Kobayashi,[2] and Kazushi Kanoda[1]

[1]*Department of Applied Physics, University of Tokyo, Bunkyo City, Tokyo 113-8656, Japan*

[2]*Department of Chemistry, College of Humanities and Sciences, Nihon University, Setagaya City, Tokyo 156-8550, Japan*

(Received 26 July 2016; revised manuscript received 23 February 2017; published 15 March 2017)

We investigated a system based solely on a single molecular species, Cu(tmdt)$_2$, accommodating d and π orbitals within the molecule. ^{13}C nuclear magnetic resonance measurements captured singlet-triplet excitations of π spins indicating the existence of a π-electron-based spin-gapped Mott insulating subsystem, which has been hidden by the large magnetic susceptibility exhibited by the d spins forming antiferromagnetic chains. The present results demonstrate a unique hybrid Mott insulator composed of antiferromagnetic and spin-singlet Mott subsystems with distinctive dimensionalities.

DOI: 10.1103/PhysRevB.95.094420

Strongly correlated electrons with orbital degrees of freedom exhibit remarkable phenomena of keen interest, as exemplified by colossal magnetoresistance and heavy fermion behavior [1–3]. Thus, finding new multiorbital systems is expected to promote the discoveries of novel phenomena and properties. It is well known that molecular conductors show various correlation-related phenomena, such as Mott transition [4], charge order/glass [5,6], spin liquid [7], and so on. However, most of the phenomena originate from a single type of orbitals, either highest occupied molecular orbital (HOMO) or lowest unoccupied molecular orbital (LUMO).

A family of materials, M(tmdt)$_2$ (tmdt = trimethylenetetrathiafulvalenedithiolate), are newly emerging molecular systems solely composed of a single molecular species in which a transition-metal ion, M, is coordinated by organic ligands, tmdt, from both sides [8,9], as shown in Figs. 1(a) and 1(b). The molecular orbitals lying near the Fermi level, ϵ_F, are the $p\pi$ orbitals extended over the tmdt ligand and the $dp\sigma$ orbital located around M [10,11]. The energy-level difference between the $p\pi$ and $dp\sigma$ orbitals can be controlled systematically by replacing M [Fig. 1(c)]. For $M =$ Ni^{2+} and Pt^{2+}, the $dp\sigma$ orbitals are of higher energy than the $p\pi$ orbitals residing around ϵ_F and the two electrons accommodated in the two $p\pi$ orbitals give $p\pi$ band semimetals with appreciable electron correlation [12–16]. Contrastingly, the $dp\sigma$ orbital lies close to the two $p\pi$ orbitals in the $M =$ Cu^{2+} system, which accommodates three electrons in the three orbitals [11]. Such intramolecular multiorbital nature with variable degeneracy differentiates M(tmdt)$_2$ from the conventional charge-transfer salts and offers a novel platform for orbital-selective physics, as demonstrated in this paper.

Cu(tmdt)$_2$ is insulating in resistivity and exhibits the magnetic susceptibility of Bonner-Fischer type with an exchange interaction $J_d = 169$ K, as shown in Fig. 1(d) [17]. A ^{1}H nuclear magnetic resonance (NMR) study revealed the characteristics of the spin dynamics of the one-dimensional antiferromagnetic Heisenberg spins in the paramagnetic state and an antiferromagnetic ordering below $T_N = 13$ K [18]. The band-structure studies suggest that the $dp\sigma$ orbitals, which are arranged one-dimensionally [see Fig. 1(b)], form a quasi-one-dimensional (Q1D) band [11,19], indicating that the $dp\sigma$ orbitals are responsible for a Q1D antiferromagnetic Mott insulator. On the other hand, theoretical studies of a multiorbital Hubbard model [19,20] predict that M(tmdt)$_2$ potentially hosts diverse magnetic and conducting states under the variations of the on-site Coulomb repulsions on the $dp\sigma$ and $p\pi$ orbitals, $U_{dp\sigma}$ and $U_{p\pi}$, respectively.

In the present study, we use the NMR technique, which is capable of probing the constituent orbital selectively, to elucidate the orbital-dependent properties in Cu(tmdt)$_2$, particularly focusing on the $p\pi$ orbital. The experiments found that the $p\pi$ orbitals constitute a spin-gapped Mott insulating subsystem, the magnetism of which was overwhelmed by the $dp\sigma$ spin component in the bulk magnetization measurement. In addition, the electron correlation in the $p\pi$ subsystem is found to be exceptionally strong among organic materials. This observation is consistent with the interpretation that Cu(tmdt)$_2$ hosts a novel multiorbital Mott insulating phase, in which very distinctive Mott insulating phases are coexistent, i.e., a Q1D antiferromagnetic subsystem and an anisotropic two-dimensional spin-gapped subsystem.

Selectively ^{13}C-enriched Cu(tmdt)$_2$ were synthesized in a similar way to the normal Cu(tmdt)$_2$, which was reported previously [17]. ^{13}C NMR measurements were performed for the fine polycrystals of ^{13}C-enriched Cu(tmdt)$_2$ under a magnetic field of 8.00 Tesla. The outers of the double-bonded carbons in the center of tmdt were selectively enriched by ^{13}C isotopes as shown in Fig. 1(a). This site has a large hyperfine coupling with the $p\pi$-electron spins. The spectra were obtained by the fast Fourier transformation of echo signals observed after the spin echo sequence, $(\pi/2)_x - (\pi)_x$.

To characterize the orbitals carrying spins in Cu(tmdt)$_2$, we first compare the ^{13}C NMR spectra of Cu(tmdt)$_2$ and a $p\pi$-orbital system Ni(tmdt)$_2$ at room temperature [Fig. 2(a)]. The shift of NMR line (δ) arises from the chemical shift (σ) and Knight shift (K) tensors (see Supplemental Material [21]). The σ depends on the local chemical structure around the nuclear site, while K reflects the spin susceptibility. For the chemical shift, we referred to the spectrum of nonmagnetic Zn(tmdt)$_2$ [Fig. 2(a)] [22,23], in which the Knight shift vanishes; thus, the isotropic chemical shift, $\sigma_{\mathrm{iso}} = 126$ ppm [shown as a gray dashed line in Fig. 2(a)], which is determined by the first moment of the spectrum, is used as the origin of the isotropic Knight shift K_{iso}. The K_{iso} of Cu(tmdt)$_2$ is negative in contrast to the positive K_{iso} value in Ni(tmdt)$_2$. This directly proves the opposite sign of the ^{13}C hyperfine coupling constant for the two compounds, namely, spins in Cu(tmdt)$_2$ and Ni(tmdt)$_2$ are accommodated in different kind

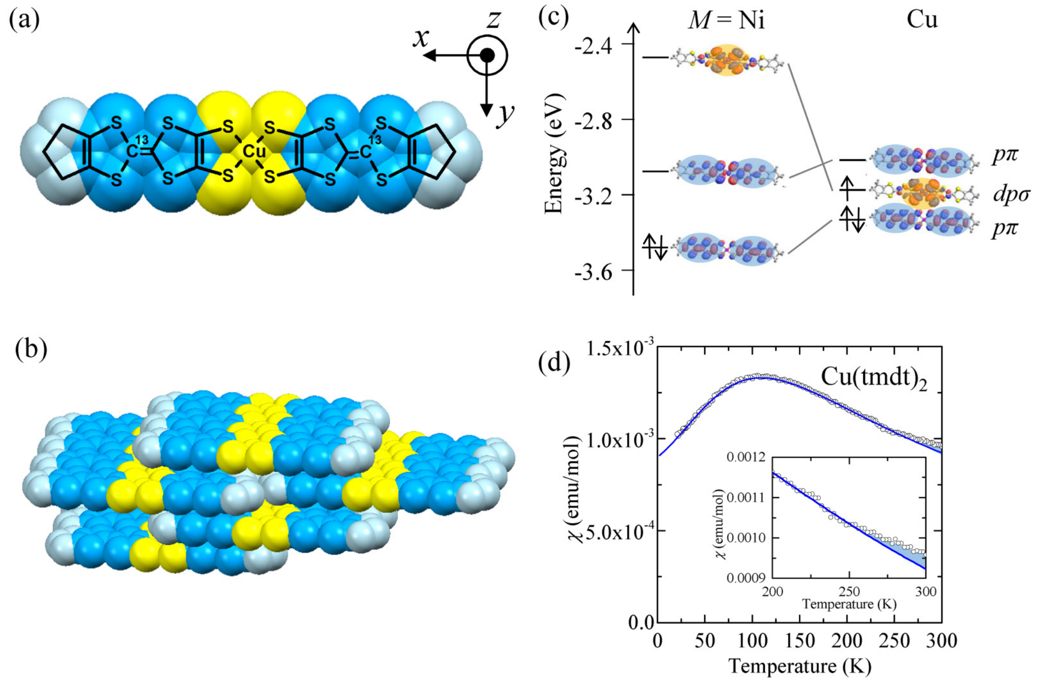

FIG. 1. Structural, orbital, and magnetic properties of Cu(tmdt)$_2$. (a) Molecular structure of Cu(tmdt)$_2$. Selectively enriched ^{13}C isotopes are labeled in the outers of the double-bonded carbons in the center of the tmdt ligands. (b) Crystal structure of Cu(tmdt)$_2$. The $dp\sigma$ orbital is populated on the central CuS$_4$ (yellow-colored part) and the $p\pi$ orbital is mainly populated in the blue-colored region in the tmdt ligand. (c) Energy levels of the $p\pi$ and $dp\sigma$ orbitals in Ni(tmdt)$_2$ and Cu(tmdt)$_2$. [10,11] (d) Temperature dependence of the spin susceptibility, which is obtained by subtracting a low-T Curie term from the raw data [17]. The blue line indicates the Bonner-Fischer-type fitting curve. The deviation of measured data from the fitted curves for $T > 250$ K is indicated as the blue region in both the main panel and the inset.

of orbitals. Because Cu(tmdt)$_2$ has narrower linewidth and larger spin susceptibility compared with Ni(tmdt)$_2$ [12,17], the former orbital should have a smaller anisotropic hyperfine coupling with the ^{13}C nuclear spin than the latter. According to the electron density calculation of M(tmdt)$_2$ [24], the $dp\sigma$ orbital has much smaller amplitude at the ^{13}C site [Fig. 1(a)] than that of the $p\pi$ orbital. Therefore, the above experimental result indicates that spins in Cu(tmdt)$_2$ mostly reside in the $dp\sigma$ orbital (with negative isotropic hyperfine coupling) unlike Ni(tmdt)$_2$ with spins accommodated in the $p\pi$ orbitals (with positive isotropic hyperfine coupling).

Figure 2(b) shows the temperature dependence of the ^{13}C NMR spectra of Cu(tmdt)$_2$. A tail extending above 200 ppm with a small fraction, which was sample dependent, is considered to originate from unknown impurity phases; so only the colored regions in the spectra are used to evaluate the Knight shift. As the temperature is decreased, the spectrum varies in its position and shape and is much broadened below 13 K, indicating an appearance of internal fields due to an antiferromagnetic transition [Fig. 2(b)]. The isotropic component of the Knight shift, $K_{\mathrm{iso}}(=\delta_{\mathrm{iso}} - \sigma_{\mathrm{iso}})$, in the paramagnetic state is plotted in Fig. 2(c). K_{iso} shows a broad peak at approximately 100 K, which coincides with the maximum of the magnetic susceptibility. If the magnetic susceptibility is normalized to K_{iso} at approximately the peak temperature, the scaling is satisfactory below the peak temperature, but fails at higher temperatures. Because the magnetic susceptibility, at least its main contribution, is explained by the Q1D $dp\sigma$ spins, the deviation implies a cancellation of K_{iso} due to an additional local field with positive ^{13}C hyperfine coupling that is especially sensed at the ^{13}C sites and develops with temperature.

^{13}C nuclear spin-lattice relaxation rate $^{13}T_1^{-1}$, which probes the dynamical spin susceptibility, is plotted in Fig. 3. The relaxation rate was determined by fitting the relaxation curve by the stretched exponential function. (For the procedure of determining the relaxation rate, see Supplemental Material [21].) The $^{13}T_1^{-1}$ shows a sharp peak at $T_{\mathrm{N}} = 13$ K and exhibits a broad minimum in the range of 30–40 K, followed by a monotonous increase that persists up to room temperature. We compare this behavior with the previously reported ^{1}H NMR T_1^{-1} ($^{1}T_1^{-1}$) in Fig. 3 [18]. The temperature dependence of $^{1}T_1^{-1}$ is consistent with the scaling theory for the one-dimensional $S = 1/2$ antiferromagnetic Heisenberg model (AFHM) [25], which has three characteristic regimes in the paramagnetic state outside of the critical region near T_{N}: (i) a low-temperature regime of 20–50 K dominated by staggered spin fluctuations, which result in a temperature-insensitive T_1^{-1} (a correction with logarithmic T dependence might appear at $T \ll J_d$, if the magnetic ordering is pushed down to far lower temperatures as in Sr$_2$CuO$_3$ [26]); (ii) an intermediate-temperature regime of 50–200 K dominated by uniform spin fluctuations (see Supplemental Material [21] for a scaling in this regime [27,28]), which result in a linear temperature dependence up to the order of the temperature of exchange interaction J_d/k_{B} (169 K in the present system); (iii) a high-temperature regime above 200 K, where spin fluctuations

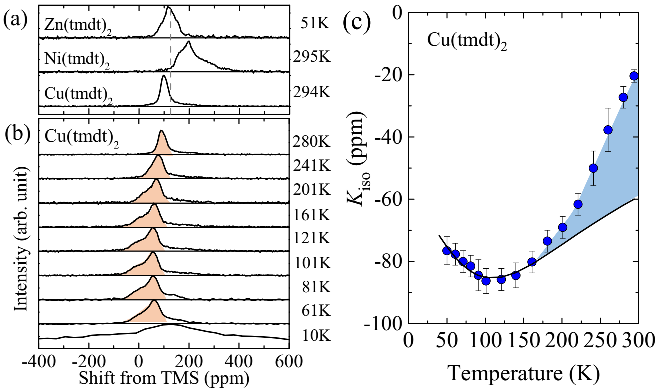

FIG. 2. ^{13}C nuclear magnetic resonance spectra and their analysis for Cu(tmdt)$_2$. (a) ^{13}C NMR spectra of Cu(tmdt)$_2$ and the $p\pi$ electron conductor Ni(tmdt)$_2$ at room temperature. The ^{13}C NMR spectrum of nonmagnetic Zn(tmdt)$_2$ at 51 K used for reference to the isotropic part of the chemical shift (a gray dashed line), $\sigma_{\rm iso}$ (=126 ppm), is also shown. (b) Temperature dependence of the ^{13}C NMR spectra for Cu(tmdt)$_2$. The colored regions in the spectra are used to determine the isotropic component of the Knight shift because tails without color are considered to originate from impurity phases. (c) Temperature dependence of the isotropic part of the ^{13}C NMR shift, $K_{\rm iso}$. The value of $K_{\rm iso}$ is determined by subtracting $\sigma_{\rm iso}$ from that of the measured NMR shift, $\delta_{\rm iso}$. The error bar is defined by the inhomogeneous width obtained in the spectral fitting (see Supplemental Material [21]). The solid curve is the magnetic susceptibility scaled to the shift values for $T < 140$ K. The colored region indicates the deviation of $K_{\rm iso}$ from the scaled magnetic susceptibility, $\Delta K_{\rm iso}$, for temperatures above 150 K, which can be attributed to the singlet-triplet excitations of the $p\pi$ spins.

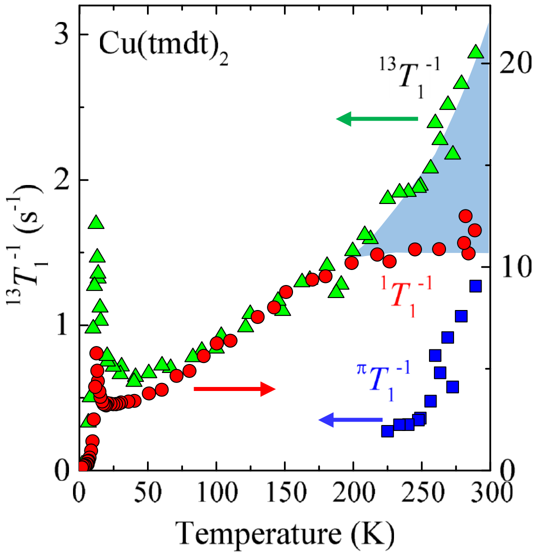

FIG. 3. Nuclear spin-lattice relaxation rate, T_1^{-1}, for Cu(tmdt)$_2$. The green triangles and the red circles indicate T_1^{-1} at the ^{13}C and ^{1}H sites (denoted as ${}^{13}T_1^{-1}$ and ${}^{1}T_1^{-1}$, respectively, in the main text). ${}^{1}T_1^{-1}$ data are from Ref. [18]. ${}^{13}T_1^{-1}$ and ${}^{1}T_1^{-1}$ are plotted so that they coincide with each other at $T = J_d$ (=169 K). The deviation of ${}^{13}T_1^{-1}$ from ${}^{1}T_1^{-1}$ normalized to ${}^{13}T_1^{-1}$ at $T = J_d$, (denoted as ${}^{\pi}T_1^{-1}$ in the text) for temperatures above 200 K, represented by the colored region, is plotted using blue squares.

with every wave numbers equally appear so that T_1^{-1} levels off. Note that the formation of a sharp peak in both of ${}^{13}T_1^{-1}$ and ${}^{1}T_1^{-1}$ at 13 K indicates the three-dimensional order due to the finite interchain exchange interactions. In Fig. 3, ${}^{13}T_1^{-1}$ and ${}^{1}T_1^{-1}$ are plotted to coincide with each other at the temperature, $J_d/k_{\rm B} = 169$ K. In regime (ii), the temperature variations of ${}^{1}T_1^{-1}$ and ${}^{13}T_1^{-1}$ are well scaled to each other. In regime (i), ${}^{1}T_1^{-1}$ is somewhat smaller in magnitude than ${}^{13}T_1^{-1}$, which can come from the difference in the form factor between the ^{13}C and ^{1}H sites; the former site is nearly exclusively hyperfine coupled to the $dp\sigma$ spins in the same molecule, whereas the latter site has appreciable hyperfine couplings to $dp\sigma$ spins in adjacent molecules as well. Thus, the antiferromagnetic fluctuations are filtered to some extent at the ^{1}H sites [18]. Most remarkably, in the regime (iii) of $T > J_d/k_{\rm B}$, ${}^{13}T_1^{-1}$ shows additional relaxation contribution that rapidly grows with temperature in contrast to the behaviors of 1D AFHM followed by ${}^{1}T_1^{-1}$.

The additional contribution to ${}^{13}T_1^{-1}$, namely a deviation of ${}^{13}T_1^{-1}$ from the scaled ${}^{1}T_1^{-1}$ value, which is approximated as 1.5 sec^{-1} for temperatures of 200–300 K (Fig. 3), is also plotted in the figure. It is evident that this additional contribution to T_1^{-1} is particularly apparent at the ^{13}C sites, indicating that the $p\pi$ spins are likely responsible for the contribution because of much stronger coupling to the ^{13}C sites than to the ^{1}H sites. This is consistent with the quasidegenerate feature of the $dp\sigma$ and $p\pi$ orbitals in Cu(tmdt)$_2$ [11,19]. Because the additional relaxation rate (denoted by ${}^{\pi}T_1^{-1}$ hereafter) appears only at high temperatures, the magnetic ground state of $p\pi$ orbitals should be nonmagnetic; then, thermally activated paramagnetic spins are observed at high temperatures. Cu(tmdt)$_2$ carries two $p\pi$ electrons for two tmdt ligands in addition to one $dp\sigma$ electron hosting the Q1D magnetism. Considering that the tmdt ligand form a dimeric arrangement with that in an adjacent molecule analogous to the β-type configuration [29] familiar for charge-transfer salts, two cases are conceivable for the $p\pi$ electronic states. One case is a band insulator, for which the band comprising the bonding orbitals in the tmdt dimers is fully occupied and has an energy gap to an unoccupied antibonding band. The other case is a dimerized Mott insulator, where one $p\pi$ electron is localized on a tmdt because of Coulomb interactions and the spins form singlets due to the dimerization.

In the case of the band insulator, the paramagnetism is due to quasiparticles being thermally activated to the upper band; thus, $(T_1T)^{-1}$ exhibits a temperature variation of the Arrhenius type (see Supplemental Material [21]). When we fit the experimental data of ${}^{\pi}T_1^{-1}$ by the form,

$$(T_1T)^{-1} \propto \exp(-\Delta/T), \tag{1}$$

a band gap of $2\Delta = 2600$ K (0.22 eV) is deduced from the activation plot of $({}^{\pi}T_1T)^{-1}$ [the inset of Fig. 4(a)]. However, such a large gap does not comply with the band-structure calculation, which predicts a vanishingly small band gap [11]. Furthermore, the magnitude of ${}^{\pi}T_1^{-1}$ is too large to explain quasiparticle excitations over the gap of 2600 K. For example, at 300 K (the temperature of one-tenth of the gap energy),

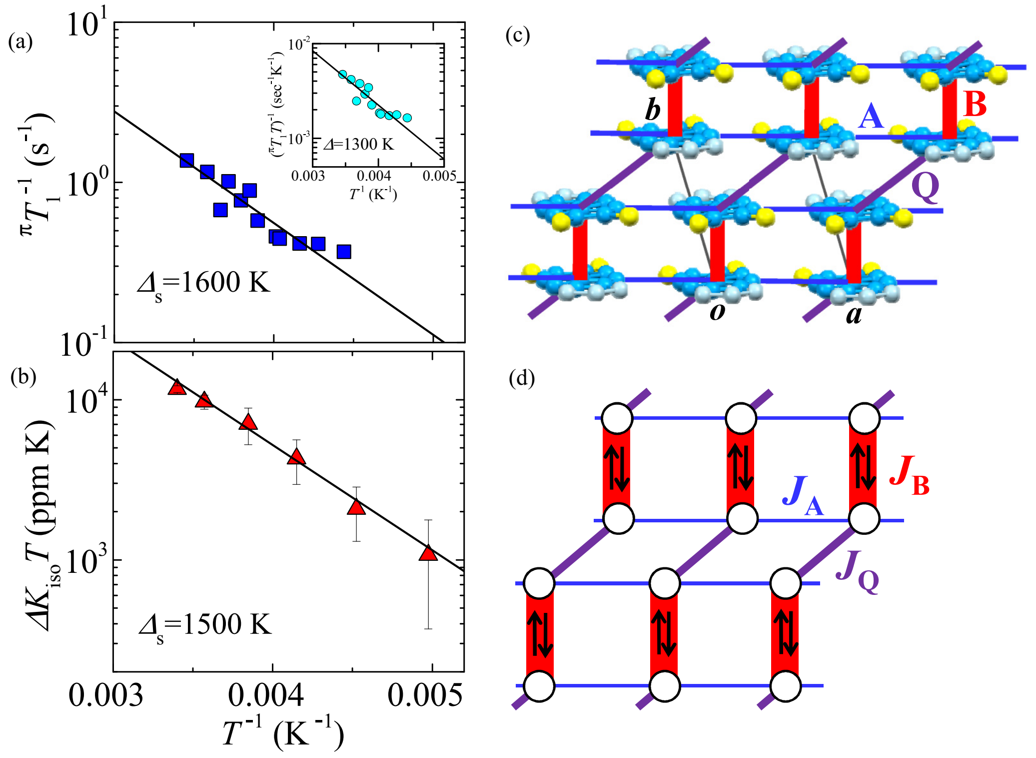

FIG. 4. NMR evidence for a spin gap and its structural reasoning for Cu(tmdt)$_2$. Activation plots for the $p\pi$-spin part of (a) ^{13}C relaxation rate, ${}^{\pi}T_1^{-1}$, and (b) the isotropic component of ^{13}C NMR shift multiplied by temperature, $\Delta K_{\mathrm{iso}}T$. The inset of (a) is the activation plot of $({}^{\pi}T_1T)^{-1}$. (c) The two-dimensional network of tmdt ligands in the *ab* plane. Bonds between the tmdt ligands with significant transfer integrals are indicated as A: [100], B: [111], and Q: [001]; the transfer integrals are $t_A = -90$ meV, $t_B = 250$ meV, and $t_Q = 134$ meV [19]. The thickness of the bonding lines is proportional to the values of the transfer integrals. (d) Spin model for the $p\pi$ electrons localized on the tmdt ligands corresponding to (c). The bonding lines are drawn such that their thickness is proportional to the exchange interaction $J_i = 4t_i^2/U_{p\pi}$ (i = A, B, and Q) with the on-site Coulomb repulsive energy $U_{p\pi}$.

the density of thermally activated quasiparticles should be several orders of magnitude smaller than the quasiparticle density in Ni(tmdt)$_2$, which has the $p\pi$-band Fermi surfaces [14]. Nevertheless, the ${}^{\pi}T_1^{-1}$ value for Cu(tmdt)$_2$ at 300 K is ~1.4 sec^{-1}, which is comparable to that for Ni(tmdt)$_2$, ~3 sec^{-1}. Therefore, the case of the $p\pi$ band insulator is ruled out.

In the case of the dimer Mott insulator, the additional relaxation originates from the singlet-triplet excitations over a spin gap of $\Delta_s = 1600$ K, which is deduced from the Arrhenius plot of ${}^{\pi}T_1^{-1}$ [the main panel of Fig. 4(a)]. The hyperfine field at the ^{13}C site from $S = 1/2$ localized $p\pi$ spins can be rather large compared to that from conducting $p\pi$ spins. According to Ref. [19], the network of tmdt ligands is two-dimensional and the largest transfer integral between the tmdt ligands is $t_B = 250$ meV [B bonds in Fig. 4(c)], which is approximately twice as large as the second largest one, $t_Q = 134$ meV [Q bond in Fig. 4(c)], and seven times larger than the intramolecular one ($t_{\mathrm{intra}} = -35$ meV). Thus, it is most likely that a spin singlet is formed in a dimer connected with the largest transfer integral, t_B.

The NMR shift shows much stronger temperature dependence than the magnetic susceptibility above 150 K [Fig. 2(c)], as we discussed before. The deviation of K_{iso} from the scaled magnetic susceptibility, ΔK_{iso}, is reasonably attributed to the singlet-triplet excitations of the $p\pi$ spins discussed above. As shown in Fig. 4(b), the shift deviation multiplied by temperature, $T\Delta K_{\mathrm{iso}}$, approximately follows the activation type of temperature dependence, $\exp(-\Delta_s/T)$ with $\Delta_s = 1500$ K, which is in general agreement with the gap value determined from ${}^{\pi}T_1^{-1}$, of 1600 K [Fig. 4(a)]. The above-obtained energy gap for the singlet-triplet excitations, $\Delta_s = 1550$ K (the average of the gap values determined from the relaxation rate and shift) enables us to calculate the $p\pi$ spin susceptibility, ${}^{\pi}\chi$, by applying the singlet-triplet excitation model, which gives

$$\chi = \frac{2N_A g^2 \mu_B^2}{3k_B T}\frac{3e^{(-\Delta_s/T)}}{1+3e^{(-\Delta_s/T)}}, \qquad (2)$$

where N_A is the Avogadro constant, g is the g factor, μ_B is the Bohr magneton, and k_B is the Boltzmann constant. Then, the magnetic susceptibility is estimated, e.g., at 280 K, to be 4.2×10^{-5} emu/mol, which explains the deviation of magnetic susceptibility from that of the Q1D $dp\sigma$ spins at the same temperature, 3.1×10^{-5} emu/mol [Fig. 1(d)] [17]. Using the hyperfine coupling constant of the $p\pi$ spins, we can also estimate ${}^{\pi}\chi$. Employing ${}^{\pi}a_{\mathrm{iso}} = 4500$ Oe/(μ_B tmdt), an average of the ${}^{\pi}a_{\mathrm{iso}}$ values for the isostructural compounds Ni(tmdt)$_2$ and Pt(tmdt)$_2$ [16], the spin susceptibility given by ${}^{\pi}\chi = {}^{\pi}a_{\mathrm{iso}}\Delta K_{\mathrm{iso}}$ is determined to be 4.3×10^{-5} emu/mol, which is in good agreement with the former two values. The spectral narrowing at higher temperatures in Cu(tmdt)$_2$

[Fig. 2(b)] is also explained by the activated $p\pi$ spins because the anisotropy in the Knight shift compensates that in chemical shift (see Supplemental Material [21]). Thus, the NMR at the ^{13}C sites captures the π-electron-based spin-gapped Mott insulator, which has been hidden behind the large $dp\sigma$ spins, and demonstrates that Cu(tmdt)$_2$ is a multiorbital Mott insulator composed of two Mott subsystems with distinctive characters in magnetism and dimensionality.

The present results provide insight into the nature of the $p\pi$ Mott insulating phase. A $p\pi$ spin model based on Fig. 4(c) is depicted in Fig. 4(d). The bond thickness is drawn so as to be proportional to the exchange interaction, J_i ($i =$ A, B, and Q). Assuming the Heisenberg type of spin coupling, the exchange interaction is given by $J_i = 4t_i^2/U_{p\pi}$, where $U_{p\pi}$ describes the on-site (tmdt) Coulomb repulsive energy. Most simply, the energy gap for the singlet-triplet excitations, Δ_s, corresponds to the largest exchange interaction, $J_{\mathrm{B}} = 4t_{\mathrm{B}}^2/U_{p\pi}$. Then, the values of $\Delta_s = 1550$ K (the average of the gap values determined from the relaxation rate and shift) and $t_{\mathrm{B}} = 250\,\mathrm{meV}$ give an estimate, $U_{p\pi} = 1.9\,\mathrm{eV}$, which is considerably higher than the U values in conventional molecular conductors (typically 1 eV or less). Taking the second largest exchange coupling, $J_{\mathrm{Q}} = 4t_{\mathrm{Q}}^2/U_{p\pi}$, the spin system is modeled to one-dimensional spin chains with J_{B}-J_{Q} alternate exchange couplings and the spin gap is given by the form of $J_{\mathrm{B}} - J_{\mathrm{Q}}/2$ according to a theoretical treatment valid for $J_{\mathrm{B}} \gg J_{\mathrm{Q}}$ [30], resulting in $U_{p\pi} = 1.6\,\mathrm{eV}$. The large $U_{p\pi}$ value is an indication of strong electron correlation in the $p\pi$ Mott phase and is explained as follows. The conventional Mott insulators in charge-transfer salts have dimeric molecular structures [31], in which a dimer plays a role of one lattice site and accommodates a hole on average. In this case, the effective on-site (dimer) U is reduced from the original U by the spatial extension of the dimer molecular orbital. The 1:1 salts would have no such reduction in the U value but maintain highly correlated nature. The tmdt subsystem in Cu(tmdt)$_2$ is in such a situation because one tmdt accommodates one carrier; i.e., the highly correlated 1:1 salt is embedded in Cu(tmdt)$_2$. This feature is common to other types of M(tmdt)$_2$, which is thus expected to generally possess the highly correlated $p\pi$ electrons. Noticeably, Au(tmdt)$_2$ and Pd(tmdt)$_2$ show antiferromagnetic orders at approximately 100 K, which is an exceptionally high transition temperature for molecular conductors [32,33].

The novel hybrid Mott insulator with intramolecular orbital selectivity substantiated in the present study provides a perspective that Cu(tmdt)$_2$ can be a unique platform for the orbital-selective Mott transition (OSMT). Because the OSMT is a key concept that underlies various attractive phenomena in multiband materials such as iron-based superconductors and heavy fermion systems, theoretical and experimental investigations in quest of novel OSMT candidates have been intensive [34–49]. The quasi-one-dimensional antiferromagnetic insulator and the anisotropic two-dimensional spin-gapped insulator residing in Cu(tmdt)$_2$ are likely to show distinctive characters in the Mott transitions and the resultant metallic phases. Synergetic phases that may emerge in sequence during the orbital-selective Mott transitions by pressure are of particular interest.

The authors thank S. Ishibashi and H. Seo for fruitful discussions. This work was supported by the JSPS Grant-in-Aids for Scientific Research (S) (Grant No. 25220709), for Challenging Exploratory Research (Grant No. 24654101), and by the JSPS Fellows (Grant No. 13J03087).

---

[1] Y. Tokura and Y. Tomioka, J. Magn. Magn. Mater. **200**, 1 (1999).
[2] E. Dagotto, T. Hotta, and A. Moreo, Phys. Rep. **344**, 1 (2001).
[3] S. Doniach, Physica B+C **91**, 231 (1977).
[4] K. Kanoda, Physica C **282–287**, 299 (1997).
[5] H. Seo, J. Phys. Soc. Jpn. **69**, 805 (2000).
[6] F. Kagawa, T. Sato, K. Miyagawa, K. Kanoda, Y. Tokura, K. Kobayashi, R. Kumai, and Y. Murakami, Nat. Phys. **9**, 419 (2013).
[7] K. Kanoda and R. Kato, Annu. Rev. Condens. Matter Phys. **2**, 167 (2011).
[8] A. Kobayashi, E. Fujiwara, and H. Kobayashi, Chem. Rev. **104**, 5243 (2004).
[9] A. Kobayashi, Y. Okano, and H. Kobayashi, J. Phys. Soc. Jpn. **75**, 051002 (2006).
[10] S. Ishibashi, K. Terakura, and A. Kobayashi, J. Phys. Soc. Jpn. **77**, 024702 (2008); **83**, 068003 (2014).
[11] S. Ishibashi and K. Terakura, Crystals **2**, 1210 (2012).
[12] H. Tanaka, Y. Okano, H. Kobayashi, W. Suzuki, and A. Kobayashi, Science **291**, 285 (2001).
[13] C. Rovira, J. J. Novoa, J. L. Mozos, P. Ordejon, and E. Canadell, Phys. Rev. B **65**, 081104(R) (2002).
[14] H. Tanaka, M. Tokumoto, S. Ishibashi, D. Graf, E. S. Choi, J. S. Brooks, S. Yasuzuka, Y. Okano, H. Kobayashi, and A. Kobayashi, J. Am. Chem. Soc. **126**, 10518 (2004).
[15] B. Zhou, A. Kobayashi, Y. Okano, T. Nakashima, S. Aoyagi, E. Nishibori, M. Sakata, M. Tokumoto, and H. Kobayashi, Adv. Mater. **21**, 3596 (2009).
[16] R. Takagi, K. Miyagawa, M. Yoshimura, H. Gangi, K. Kanoda, B. Zhou, Y. Idobata, and A. Kobayashi, Phys. Rev. B **93**, 024403 (2016).
[17] B. Zhou, H. Yajima, A. Kobayashi, Y. Okano, H. Tanaka, T. Kumashiro, E. Nishibori, H. Sawa, and H. Kobayashi, Inorg. Chem. **49**, 6740 (2010).
[18] R. Takagi, K. Miyagawa, K. Kanoda, B. Zhou, A. Kobayashi, and H. Kobayashi, Phys. Rev. B **85**, 184424 (2012).
[19] H. Seo, S. Ishibashi, Y. Otsuka, H. Fukuyama, and K. Terakura, J. Phys. Soc. Jpn. **82**, 054711 (2013).
[20] H. Seo, S. Ishibashi, Y. Okano, H. Kobayashi, A. Kobayashi, H. Fukuyama, and K. Terakura, J. Phys. Soc. Jpn. **77**, 023714 (2008).
[21] See Supplemental Material at http://link.aps.org/supplemental/10.1103/PhysRevB.95.094420 for details of the analyses.
[22] K. Yamamoto, E. Fujiwara, A. Kobayashi, Y. Fujishiro, E. Nishibori, M. Sakata, M. Takata, H. Tanaka, Y. Okano, and H. Kobayashi, Chem. Lett. **34**, 1090 (2005).
[23] H. Gangi, R. Takagi, K. Miyagawa, K. Kanoda, B. Zhou, and A. Kobayashi (unpublished).

[24] S. Ishibashi (private communication).
[25] S. Sachdev, Phys. Rev. B **50**, 13006 (1994).
[26] V. Barzykin, Phys. Rev. B **63**, 140412(R) (2001).
[27] C. Bourbonnais, P. Wzietek, F. Creuzet, D. Jérome, P. Batail, and K. Bechgaard, Phys. Rev. Lett. **62**, 1532 (1989).
[28] P. Wzietek, C. Bourbonnais, F. Creuzet, D. Jérome, and K. Bechgaard, Europhys. Lett. **12**, 453 (1990).
[29] T. Mori, Bull. Chem. Soc. Jpn. **71**, 2509 (1998).
[30] K. Hida, Phys. Rev. B **45**, 2207 (1992).
[31] K. Kanoda, J. Phys. Soc. Jpn. **75**, 051007 (2006).
[32] Y. Hara, K. Miyagawa, K. Kanoda, M. Shimamura, B. Zhou, A. Kobayashi, and H. Kobayashi, J. Phys. Soc. Jpn. **77**, 053706 (2008).
[33] S. Ogura, Y. Idobata, B. Zhou, A. Kobayashi, R. Takagi, K. Miyagawa, K. Kanoda, H. Kasai, E. Nishibori, C. Satoko, and B. Delley, Inorg. Chem. **55**, 7709 (2016).
[34] V. I. Anisimov, I. A. Nekrasov, D. E. Kondakov, T. M. Rice, and M. Sigrist, Eur. Phys. J. B **25**, 191 (2002).
[35] A. Koga, N. Kawakami, T. M. Rice, and M. Sigrist, Phys. Rev. Lett. **92**, 216402 (2004).
[36] L. de' Medici, A. Georges, and S. Biermann, Phys. Rev. B **72**, 205124 (2005).
[37] M. Ferrero, F. Becca, M. Fabrizio, and M. Capone, Phys. Rev. B **72**, 205126 (2005).
[38] A. Liebsch, Phys. Rev. Lett. **95**, 116402 (2005).
[39] K. Inaba and A. Koga, Phys. Rev. B **73**, 155106 (2006).
[40] L. de' Medici, S. R. Hassan, M. Capone, and X. Dai, Phys. Rev. Lett. **102**, 126401 (2009).
[41] H. Lee, Y.-Z. Zhang, H. O. Jeschke, and R. Valentí, Phys. Rev. B **84**, 020401(R) (2011).
[42] Y.-Z. Zhang, H. Lee, H.-Q. Lin, C.-Q. Wu, H. O. Jeschke, and R. Valentí, Phys. Rev. B **85**, 035123 (2012).
[43] L. Huang, L. Du, and X. Dai, Phys. Rev. B **86**, 035150 (2012).
[44] L. de' Medici, A. Georges, G. Kotliar, and S. Biermann, Phys. Rev. Lett. **95**, 066402 (2005).
[45] C. Pepin, Phys. Rev. Lett. **98**, 206401 (2007).
[46] L. De Leo, M. Civelli, and G. Kotliar, Phys. Rev. Lett. **101**, 256404 (2008).
[47] M. Yi, D. H. Lu, R. Yu, S. C. Riggs, J.-H. Chu, B. Lv, Z. K. Liu, M. Lu, Y.-T. Cui, M. Hashimoto, S.-K. Mo, Z. Hussain, C. W. Chu, I. R. Fisher, Q. Si, and Z.-X. Shen, Phys. Rev. Lett. **110**, 067003 (2013).
[48] S. Mukherjee, N. F. Quackenbush, H. Paik, C. Schlueter, T.-L. Lee, D. G. Schlom, L. F. J. Piper, and W.-C. Lee, Phys. Rev. B **93**, 241110(R) (2016).
[49] E. Civardi, M. Moroni, M. Babij, Z. Bukowski, and P. Carretta, Phys. Rev. Lett. **117**, 217001 (2016).